ChemCatChem

Research Article
doi.org/10.1002/cctc.202301111

Chemistry Europe
European Chemical Societies Publishing

www.chemcatchem.org

One-Step Synthesis of Air-Stable Sulfur-Doped Molybdenum Phosphide Catalyst

Song Tian,[a] Wei Mao,[a] Donghuai Tu,[a] Yanbo Bai,[a] Zhaohua Jia,[a] Yue Qin,[a] Xiang Li,[b] Anjie Wang,[c] Jimmy A. Faria Albanese,[d] and Jian Lu*[a]

Transition-metal phosphides prepared from temperature-programmed reduction (TPR) are generally known to be unstable and prone to surface structure decomposition upon exposure to air. In this work, air-stable molybdenum phosphide (MoP) was prepared using TPR modified by sulfur. This catalyst was exposed to ambient atmosphere for up to 150 days and still maintained its surface and bulk structures as the fresh sample derived from in situ reduction. The metal phosphosulfide phase generated during TPR not only contributes to the solid structural properties but also exhibits superior catalytic activity in various hydrofining reactions compared to traditional MoP catalysts. Additionally, this preparation strategy was used to synthesize other sulfur-doped metal phosphides, such as CoP and Cu_3P. Both of these catalysts exhibited excellent air-stability.

Introduction

The covalent and metallic characters of metal-rich transition-metal phosphides (TMPs) capture more and more attention in recent years.[1] They manifest high activity and stability under hydrogenating and oxygen-free reactions, and are promising for a variety of important hydrofining reactions.[2] Recently, they are also reported to display attractive performances in electrochemistry,[3] methanol synthesis[4] and photocatalysis.[5] TMPs, synthesized using conventional TPR, are highly pyrophoric and prone to oxidation when exposed to air, leading to deteriorated catalytic properties.[6] This limits their ex situ applications, such as in photochemical and electrochemical processes,[7] to oxygen-free environments. To promote the practical application of TMPs, a strategy to protect the structure of TMPs against oxidation in an oxygen-containing environment and provide satisfactory catalytic performance is highly desired.

The most common strategy to improve the stability of TMPs prepared via TPR in air is to generate a protective layer by surface passivation using a diluted O_2 flow,[6a] which slows or prevents further oxidation of the underlying metal atoms. Afterward, upon contacting with H_2 again, the protective layer is re-reduced to metal phosphide before catalytic application. However, the P–O bonds of TMPs surface built during passivation by a diluted O_2/Ar can be scarcely recovered, resulting in unsatisfactory recovery of their application properties. In optoelectronic devices and photovoltaics, $(NH_4)_2S$ or H_2S is often used to passivate III–V semiconductors like InP and GaP.[8] It has been reported that Ni_2P/MCM-41 treated by H_2S passivation showed comparable activity to the fresh sample prepared via the in situ reduction method.[9] The activity loss of the catalyst was minor even after being exposed to air for 150 days. The possible reason is that metal phosphate precursors likely interact with H_2S to produce amorphous sulfide species and phosphide crystals in the presence of hydrogen sulfide at high temperature, maintaining the stability of P species in subsequent reduction.[10] Several studies[3a,11] have observed that when TMPs are passivated by H_2S, their surface structure is modified, forming a metal phosphosulfide phase that enhances the air-stability of TMPs. Moreover, the formed phosphosulfide phase can also promote the catalytic activity of TMPs in hydrogenation[12] and electrochemical[3a] reactions. These results demonstrate the feasibility and importance of sulfur modification for the air-stability and catalytic behavior of TMP catalysts. However, H_2S passivation treatment is tedious and needs to be performed carefully, and is not environmentally friendly due to the corrosive and toxic properties of H_2S. Consequently, developing a facile and practical approach of introducing sulfur into TMPs structure is still highly pursued.

Our previous study presented an alternative approach for synthesizing Ni_2P by reducing nickel hexathiodiphosphate ($Ni_2P_2S_6$).[13] The reduction of the precursor released sulfur

[a] S. Tian, W. Mao, D. Tu, Y. Bai, Z. Jia, Y. Qin, Prof. J. Lu
State Key Laboratory of Fluorine & Nitrogen Chemicals
Xi'an Modern Chemistry Research Institute
Xi'an, Shaanxi 710065 (P. R. China)
E-mail: lujian204@gmail.com

[b] Prof. X. Li
Tianjin Key Laboratory of Brine Chemical Engineering and Resource Eco-utilization
College of Chemical Engineering and Materials Science
Tianjin University of Science and Technology
Tianjin 300457 (P. R. China)

[c] Prof. A. Wang
State Key Laboratory of Fine Chemicals
School of Chemical Engineering
Dalian University of Technology
Dalian 116024 (P. R. China)

[d] Prof. J. A. Faria Albanese
Catalytic Processes and Materials Group
Faculty of Science and Technology
MESA + Institute for Nanotechnology
University of Twente
7500 AE, Enschede (The Netherlands)

Supporting information for this article is available on the WWW under https://doi.org/10.1002/cctc.202301111

species, which formed a sulfur-containing layer on the catalyst surface, leading to higher catalytic activity in hydrodesulfurization (HDS) and selective hydrogenation reactions. However, we did not investigate the air-stability of the prepared samples. In this work, our goal is to extend the application of this method to synthesize metal phosphides via reduction of thiophosphate precursors and, more importantly, to determine the air-stability of the resulting S-doped phosphide catalysts and their performance in ex and in situ hydrofining reactions.

MoP adopts the hexagonal tungsten carbide (WC) structure type (P_{6m2}).[14] Due to the large radius of P, the strength of Mo is reduced when it enters the metal lattice, leading to the instability of the lattice structure.[15] Therefore, during the process of HDS, the surface structure of MoP can be reconstructed faster than that of Ni_2P, resulting in the formation of a sulfur-containing layer on the catalyst surface.[11a] The S-modified MoP facilitates the adsorption of reactants and reduces the energy barrier, leading to an increase in the reaction.[12] Although the positive effect of sulfur on MoP has been verified in a large number of experiments, the rate of sulfur uptake is too high for direct formation of the sulfur-containing molybdenum phosphides active phase. Herein, we directly obtain molybdenum phosphosulfide by facile one-step reduction of the thiophosphate precursor, with the introduction of sulfur during reduction used as the key to explore the mechanism of improved activity and stability of the catalyst.

Table 1. Expressions of different molybdenum phosphide names.

Names	Expression
MoP-S	Reduction from sulfur-containing precursor
MoP-T	Reduction from phosphate precursor
MoP-T-S	Passivated by H_2S after reduction of MoP-T

Results and Discussion

The sulfur-containing precursor initially had an amorphous structure (Figure S1). However, after being treated in a tubular reactor at 450 °C, 0.1 MPa H_2, and a flow rate of 100 mL min^{-1} for 2 h, the precursor exhibited diffraction peaks. Those peaks were observed at 32.2°, 43.2° and 57.5°, respectively, corresponding to the characteristic diffraction peaks of MoP phase (PDF card 74-1385).[16] Furthermore, higher reduction temperatures ranging from 500 to 650 °C were investigated, but they only resulted in the formation of MoP phase, regardless of the temperature. The reduction of the sulfur-containing precursor to MoP occurred after 4 hours at 450 °C (Figure S2), which was 200 °C lower than the temperature required by the conventional TPR method.

The XRD patterns did not show any diffraction peaks corresponding to sulfur, but the average particle size of MoP-S (61 nm) (Table 1) estimated from the XRD pattern was smaller than that of MoP-T (237 nm) (Table 1 and Table S2). In the high-resolution transmission electron microscopy (HRTEM) image of the MoP-S sample (Figure 1), clear lattice fringes with interplane distances of 2.13 Å and 2.84 Å were observed, corresponding to the (101) and (100) planes of MoP, respectively, confirming the formation of the MoP phase. On the other hand, MoP-T and MoP-T-S (Table 1) showed similar lattice spacing (Figure 1), which closely matched the values in the PDF card (2.09 Å and 2.78 Å). The slightly larger lattice spacing observed in MoP-S is likely due to the presence of sulfur atoms incorporated into the MoP structure, indirectly indicating its difference from the structure of MoP-T-S. Additionally, TEM-mapping (Figure S3) revealed a nearly homogeneous distribution of numerous sulfur atoms (11.9 at. %) on MoP-S surface.

The XPS spectra in Mo 3d, P 2p, and S 2p regions for MoP-S and MoP-T are presented in Figure 2. All samples were passivated in a flow of a 0.5 mol% O_2/Ar prior to exposure to

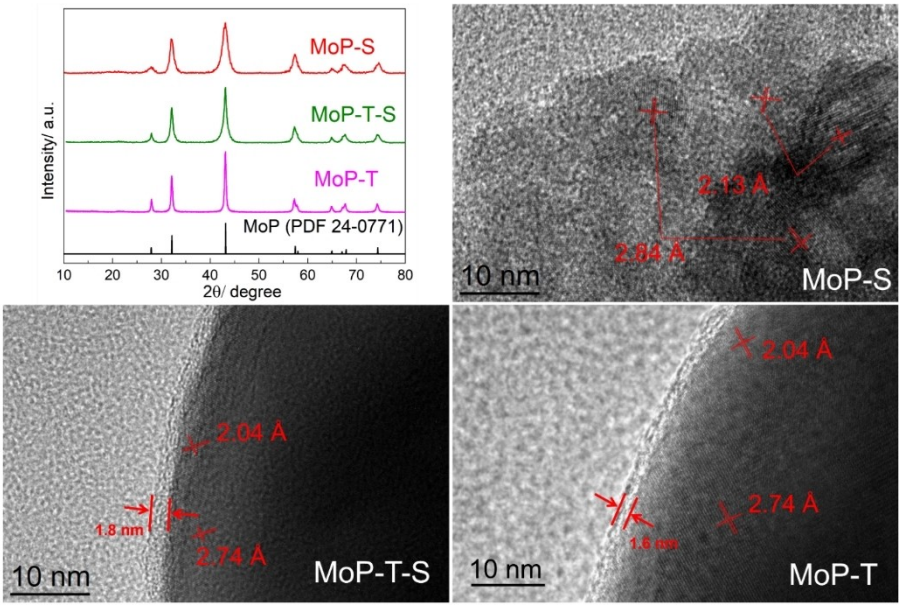

Figure 1. XRD patterns and HRTEM images of different MoP samples.

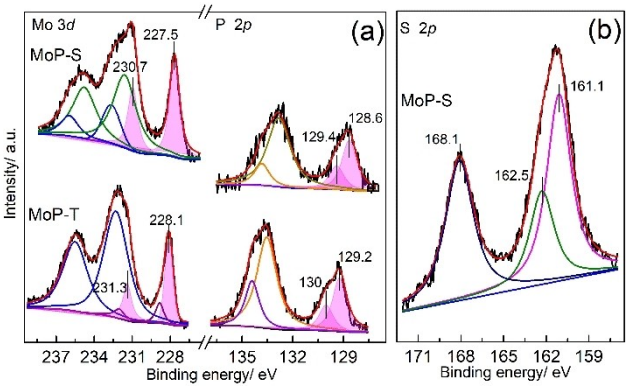

Figure 2. XPS spectra of the MoP-S and MoP-T in the Mo 3d, P 2p (a) and S 2p (b) region.

air, which explains the presence of molybdenum and phosphorus oxide species in the spectra. The assignment of the oxidation states and reduction states of different Mo species is based on the Mo ($3d_{3/2,\ 5/2}$) spin-orbit components, which have a separation of 3.2 eV and equal FWHM.[17] In the case of MoP-T, the doublet observed with a separation of 3.3 eV, located at 231.3 and 228.1 eV, corresponds to $Mo^{\delta+}$ species ($0<\delta<4$),[18] which are commonly associated with molybdenum species in MoP. These $Mo^{\delta+}$ species contribute to only 17% of the fitting peaks. Another two doublets observed at 235.5 and 232.2 eV can be attributed to Mo^{6+},[16] while 232 and 228.8 eV are assigned to Mo^{4+}.[19] The P species on the surface of MoP-T, bonded to Mo in the form of a phosphide,[18] appear as a doublet at 130 and 129.2 eV in the P ($2p_{1/2,\ 3/2}$) region. Additionally, the oxidation states of P at 133.5 and 134.4 eV correspond to PO_4^{3-}[3a] and P_2O_5,[20] respectively. For MoP-S, the Mo 3d region also exhibits a mixture of Mo oxidation states, including Mo^{6+} species at 235.7 and 232.5 eV,[16] and Mo^{5+} species at 234.6 and 231.4 eV.[21] Peak fitting analysis reveals that approximately 30% of the Mo signal corresponds to Mo–P bonding,[18] which is shifted to 230.7 and 227.5 eV, about 0.6 eV lower than that of MoP-T. A similar downward shift is observed in the corresponding P species, with fitting peaks at 129.4 and 128.6 eV.[18] The oxidative P species on the MoP-S surface appear at 133.8 eV and can be attributed to PO_4^{3-} species.[3a]

The XPS analysis reveals the presence of sulfur on the surface of MoP-S catalyst (Figure 2b), which is consistent with the TEM-mapping results (Figure S3). The S 2p peak can be deconvoluted into two Gaussian peaks at 161.1 and 162.5 eV, corresponding to sulfide species (S^{2-}) and thiolate-type environment,[18] respectively. These sulfur species are similar to those observed on the surface of a bulk MoP catalyst after the HDS reaction[22] or a molybdenum phosphosulfide.[9] Additionally, a peak at a higher binding energy of 168.1 eV indicates the presence of surface sulfate species, such as SO_4^{2-}.[23]

The surface S/P/Mo atomic ratio of the fresh MoP-S catalyst, estimated by XPS, is found to be 0.39/2.14/1 (Table 2). This indicates that the surface of the fresh MoP-S catalyst is phosphorus-rich compared to the stoichiometric value of 1.0. This higher phosphorus content is likely due to the abundant presence of phosphorus in the precursor. XRF results show that the S/P/Mo atomic ratios for MoP-S and MoP-T are 0.33/0.89/1 and 0/0.92/1, respectively. This suggests that, in theory, 1/10 of the phosphorus in the MoP-S sample is replaced by sulfur. Furthermore, the surface S/Mo ratio (0.39) is nearly the same as the bulk value (0.33) (Table 2), indicating that sulfur is homogeneously incorporated into the bulk of the MoP-S catalyst.

The observed shift of the binding energies (approximately 0.6 eV) of Mo and P species in MoP-S to lower values compared to MoP-T (Figure 2) indicates strong electronic interactions between sulfur and the surface MoP species, as discussed below. In our previous work,[13] we found that the presence of sulfur on the surface of Ni_2P is attributed to the incorporation of sulfur released from H_2S during the reduction of $Ni_2P_2S_6$. Similarly, MoP-S, which has a high sulfur content (S/Mo = 0.89) in the precursor without undergoing calcination (Table 2), can release sufficient H_2S during reduction to combine with Mo and P. Furthermore, a distinct peak observed at approximately 132.7 eV corresponds to the binding energy of P in a P–S group[24] (Figure 2b). These findings collectively suggest that sulfur is likely incorporated into the MoP crystal lattice, forming a molybdenum phosphosulfide phase.

It has been postulated that sulfidation of TMPs following reduction leads to the formation of a phosphosulfide layer,[11a] which is believed to be the active site in various hydrogenation reactions.[11b] Additionally, molybdenum phosphosulfide catalysts have been shown to exhibit exceptional activity and stability for the hydrogen evolution process in acidic environments.[3a] In this study, we investigated the performance of MoP-S and MoP-T catalysts in the in situ HDS of dibenzothiophene (DBT) and hydrodechlorination (HDC) of chlorodifluoromethane ($CHClF_2$).

Typically, the HDS of DBT proceeds via two parallel routes,[11b] as illustrated in Scheme S1: the direct desulfurization

Table 2. XPS, XRF and BET results if different samples.

Catalysts	XRF		XPS		Surface area/$m^2\,g^{-1}$
	P/Mo	S/Mo	P/Mo	S/Mo	
MoP-S precursor	2.32	0.89	–	–	–
MoP-S	0.89	0.33	2.14	0.39	25.1
MoP-T	0.92	–	1.66	–	13.1
MoP-T spent[25]	1.03	0.045	1.37	0.35	–

(DDS) route, which yields biphenyl (BP), and the hydrogenation (HYD) route, which generates sulfur-containing intermediates such as tetrahydro, hexahydro, and dodecahydro that are subsequently desulfurized to form cyclohexylbenzenes and bicyclohexyls. Therefore, the selectivity towards biphenyl can be used as a measure of the DDS activity, as the hydrogenation of biphenyl to cyclohexylbenzenes is minimal in the presence of sulfur-containing compounds. The quantity ($1\text{-}S_{BP}$) represents the contribution of the HYD pathway. Table 3 reveals that the conversion of DBT over MoP-S was more than twice as high as that over MoP-T. Furthermore, the HYD pathway selectivity for MoP-S was 60.1%, which was 13% higher than that for MoP-T. These results suggest that the enhanced HDS activity of the molybdenum phosphosulfide phase strongly promotes the HYD pathway over the DDS pathway.

The data for MoP-T presented in Table 3 were evaluated after a duration of six hours. Further extension of the reaction time to 35 hours showed a 4–5% improvement in DBT conversion (Figure S4). Meanwhile, the BP selectivity exhibited similar curves along with the increasing reaction time, suggesting a positive influence of sulfur on MoP-T and the DDS activity. Similar observations were reported by Bussell et al.[16] and Bai et al.,[11a,25] where the HDS of DBT over fresh MoP resulted in increased DBT conversion and a subsequent stabilization of BP selectivity over time. This phenomenon was attributed to the generation of new active sites on the bulk MoP, likely arising from the surface incorporation of sulfur during the HDS reaction. In contrast, the performance of MoP-S remained largely unaffected by prolonged reaction time. The selectivity of the HYD pathway was consistently above 50% and remained constant regardless of the reaction time, indicating that the HYD pathway was significantly more facilitated than the DDS pathway in enhancing the HDS activity of the molybdenum phosphosulfide phase. The combined results suggest that the phosphosulfide phase used in MoP-S, synthesized via sulfur doping, is distinct from the phase reconstructed during the HDS reaction on MoP-T.

In the HDC of $CHClF_2$, the cleavage of C–Cl bond is known to be the rate-determining step, making it a structure-sensitive reaction.[26] The conversion of $CHClF_2$ over MoP-S was nearly 3.5 times as high as that over MoP-T. Interestingly, both catalysts exhibited similar selectivity towards the target product. The continuous hydroconversion of $CHClF_2$ over molybdenum phosphide may indeed be constrained by the intrinsic hydrogen activation ability of the catalyst.[27] As evidenced by Table S3, compounds such as CH_4 and CH_3F were detected in the product, although their selectivity was not high. This observation may be attributed to the fact that C–F bonds (451 kJ/mol) can be stronger than C–Cl (349 kJ/mol) bond. Therefore, to conduct a more comprehensive comparison of the catalytic performance of the two catalysts, it is crucial to calculate the HDC turnover frequency (TOF) for each catalyst, taking into account their different particle sizes. However, the conversion of $CHClF_2$ over MoP-S was too high to enable a reasonable comparison. Therefore, the relative HDC reaction rates of the two catalysts were calculated based on their surface areas, contact time, and the corresponding $CHClF_2$ conversions [Equation (1)]:

$$\text{Relative rate} = \eta_{converted}/(T_{contact\ time} \times W_{cat.} \times S_g) \quad (1)$$

where $\eta_{converted}$ is the reactant conversion, mol; and S_g is the surface area of the catalyst, m^2/g. These calculations will provide a more accurate assessment of the HDC activity of MoP-S compared to MoP-T, accounting for the differences in particle size and ensuring a fair comparison between the two catalysts. The results (Table 3) indicate that the MoP-S has higher intrinsic dechlorination activity than MoP-T. The excellent properties on the activity of MoP-S is further confirmed by the relative HDS reaction rates (Table 3). The value of MoP-S (1.3×10^{-3} mol m^{-2} h^{-1}) was about 1.8 times as high as that of MoP-T (0.7×10^{-3} mol m^{-2} h^{-1}).

In the context of the sulfur-doped molybdenum phosphosulfide phase, the sulfur content is directly derived from the precursor. TEM imaging (Figure 1) confirms the absence of a distinct oxidation layer encasing the crystal particles, and the lattice structure remains consistent with the bulk material. Moreover, the introduction of sulfur can lead to a redistribution of surface charges on MoP-S. The negatively shifted P 2p peaks bonded to Mo, along with the appearance of peak associated with P–S bonds (Figure 2), indicates the sharing of electrons between P and the more electronegative S atoms.[3a,28] The interplay of electronic properties between P and S gives rise to a novel non-metallic grouping that acts in synergy with Mo,[29] leading to a reduction in its electronic binding energy. The former covalent state of Mo tends to become more metallic,[30] thus forming an active catalyst phase[3a] and contributing to the exceptional performance of MoP-S. Additionally, the presence of reduced Mo species on the surfaces of both MoP-S (30%) and MoP-T (17%) illustrates that the introduction of S atoms can hinder the oxidation of MoP.[6b] Consequently, the surface of MoP-S exhibits a more inert oxidation behavior compared to MoP-T. For a comprehensive understanding of air tolerance and structure-performance relationships of these distinct phosphosulfide phases, conducting a meticulous experimental study is essential.

We conducted the HDC of $CHClF_2$ using unpassivated MoP-S samples after reduction, which were directly exposed to air for 0 day (MoP-S0), 30 days (MoP-S30) and 150 days (MoP-S150). Similarly, the MoP-T samples after H_2S passivation were also exposed to air for the equivalent durations, referred to as MoP-T-S0, MoP-T-S30 and MoP-T-S150, respectively. The experimental tube heated directly to the target temperature under the H_2

Table 3. The catalytic performances of MoP-S and MoP-T.

Reaction	Conversion/%		Selectivity/%		Relative rate/ mol m^{-2} h^{-1}	
	MoP-S	MoP-T	MoP-S	MoP-T	MoP-S	MoP-T
HDS	59.3	29.7	60.1[a]	47.3[a]	1.3×10^{-3}	0.7×10^{-3}
HDC	88.1	27.5	75.1[b]	71.2[b]	0.025	0.014

[a] HYD pathway selectivity, $(1\text{-}S_{BP})\times100$%. [b] CH_2F_2 selectivity.

atmosphere. MoP-S has already exhibited a high $CHClF_2$ conversion under the currently reaction conditions (Table 3). To ensure accurate performance evaluation without issues arising from excessively high loading, we assessed this HDC activity of all catalysts at two different GHSV (3600 h^{-1} and 900 h^{-1}). The results (Figure 3) of the reactions demonstrated the following trends:

Common Trends for MoP-S and MoP-T: 1) At the initial high GHSV stage, all exposed catalysts displayed an induction period, the length of which was directly proportional to the duration of exposure. Subsequently, their activity recovered to a level similar to that of the 0d catalysts. Moreover, when the reaction switched to the low GHSV stage, no induction periods were observed. This indicated the complete elimination of activity impact caused by air exposure. 2) High GHSV led to low conversion but high selectivity. Conversely, low GHSV resulted in high conversion but low selectivity.

Distinctive Behavior for MoP-S and MoP-T: As for MoP-S, returning to the second high GHSV stage led to a revival of activity levels seen in the first stage. Throughout this stage, no changes occurred in either conversion or selectivity over the reaction time. This stable performance suggests that the structure of MoP-S remained consistent regardless of air exposure or duration. In contrast, the activity of MoP-T samples exposed to air for extended periods decreased during the third stage. These values gradually decreased with increasing air exposure time. $CHClF_2$ conversion continued to decline with increasing reaction time, indicating catalyst deactivation. This observation implied that MoP-T catalysts, even with H_2S post-treatment, were significantly influenced by air in terms of structural stability.

The induction period observed in MoP-S during the initial high GHSV stage of the reaction might suggest surface oxidation when the catalyst was exposed to air. However, XPS characterization results of the fresh MoP-S150 catalyst (Figure S5) did not reveal any binding energy peaks associated with Mo–O and P–O bonds. Further SEM-EDX analysis(Figure S6) demonstrated a significant reduction in the oxygen content on the catalyst surface, decreasing from 7.6 at.% before the reaction to 2.8 at.% after the reaction. This reduction implies that most of the oxygen on the surface is physically adsorbed oxygen. As the hydrogenation reaction progresses, the weak oxidation behavior on the surface diminishes, and the reaction activity returns to the level observed with an unexposed catalyst.

The ex situ hydrogenation of nitrobenzene over different MoP-S and MoP-T samples (Figure 4) further confirmed our findings. Initially, when comparing the relatively fresh samples that were promptly placed in the setup after reduction, MoP-S exhibited more than double the conversion of reactant compared to MoP-T-S (54.1% and 21.8%, respectively), and even three times higher than MoP-T (16.1%, the MoP-T sample without passivation). Additionally, MoP-S showed a slightly higher selectivity towards aniline. MoP-T catalysts treated with H_2S passivation demonstrated higher activity compared to those without passivation, but the samples exposed to air for an extended period displayed decreased performance (Figure 4). This decrease in activity correlates with the gradual thickening of the oxide layer observed in the TEM results (Figure 5). EDX analysis (Figure S7) reveals a notable presence of oxygen on the catalyst surface, while XPS results (Figure S5) demonstrate significant oxidation reactions have occurred on Mo, P, and S on the surface of MoP-T-S150. These findings provide direct evidence that the incorporation of sulfur in MoP-

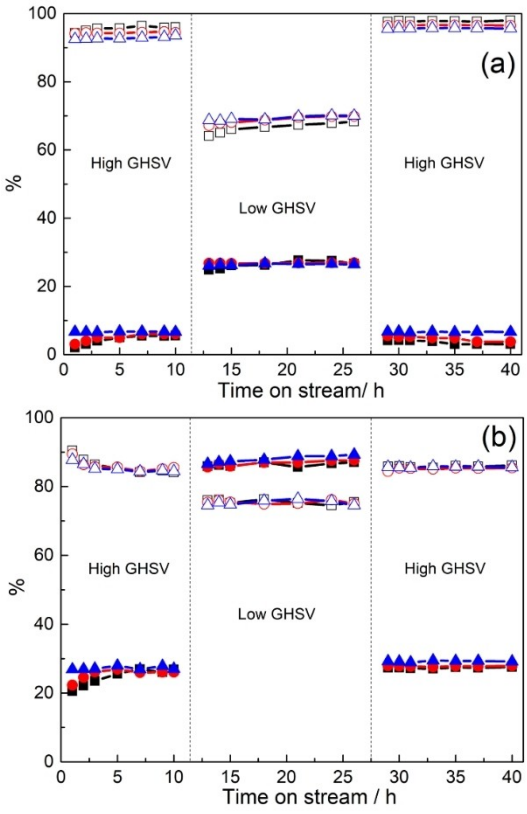

Figure 3. Variation of $CHClF_2$ conversion and CH_2F_2 selectivity during HDC at 300 °C over MoP-T(a) and MoP-S(b) catalyst post-reduced different time (solid for the conversion and open for the selectivity, blue for 0d, red for 30d and black for 150d).

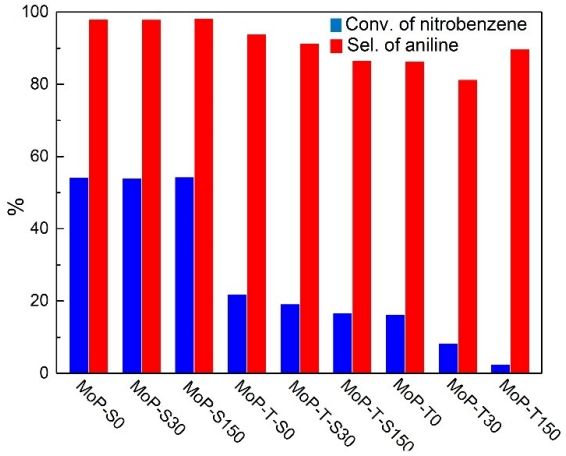

Figure 4. Variation of nitrobenzene conversion and aniline selectivity at 50 °C over different catalysts.

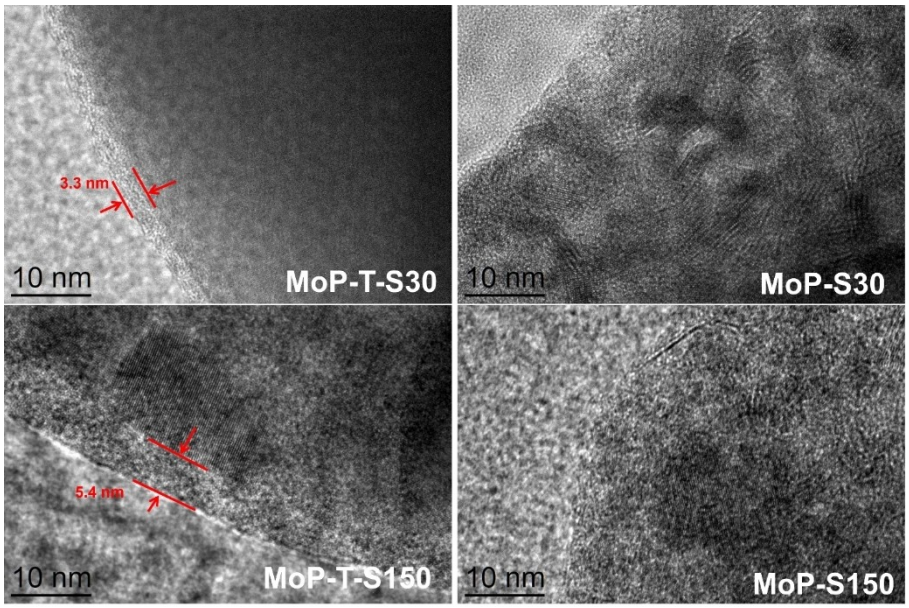

Figure 5. TEM images of different MoP-T and MoP-S samples.

T can indeed slow down the oxidation process. However, it is important to note that the issue of air-sensitivity is not fundamentally resolved by this method. In contrast, the performance of MoP-S30 and MoP-S150 catalysts did not exhibit any loss. Moreover, the TEM profiles of those MoP-S samples showed minimal changes (Figure 5) and hardly noticeable changes can be seen from the XRD (Figure S8). The XPS spectra of MoP-S150 and MoP-T-S150 also showed a more intuitive difference in their oxidation states (Figure S5). Both the Mo–O and P–O bond were hardly detected in the surface of MoP-S150. The above results indicate that the crystal structure remained unchanged during direct exposure to air treatment.

Sulfur has been detected in both the surface and bulk of MoP prepared through sulfidation-reduction procedures; however, these catalysts still exhibit susceptibility to air.[10] TMPs passivated with H_2S have shown superior activity compared to those passivated with O_2, and their performance is comparable to in-situ reduction catalysts.[9] Nevertheless, the preparation of such catalysts still requires high-temperature reduction. In this work, the role of sulfur is distinct from the aforementioned cases. H_2S generated during the reduction of the sulfur-containing precursor or directly introduces sulfur into the MoP crystal, resulting in the formation of the molybdenum phosphosulfide phase at a lower temperature of 450 °C. Importantly, this catalyst exhibits outstanding catalytic performance and shows insensitivity to air, distinguishing it from catalysts prepared using the conventional TPR method. This discovery enables more efficient preparation and utilization of TMPs.

To further demonstrate the applicability of this method for synthesizing metal phosphides, we applied the same approach to synthesize other metal phosphides. Figure S9 illustrates the successful synthesis of CoP and Cu_3P crystals through H_2 reduction of sulfur-containing precursors. The XRD patterns of the synthesized samples did not show any additional peaks corresponding to impurities, and the TEM images revealed no significant presence of amorphous layers in the samples that were exposed to air for 150 days. These results provide compelling evidence that highly air-insensitive metal phosphides can be easily and flexibly synthesized through a one-step reduction of sulfur-containing precursors.

Conclusions

The molybdenum phosphosulfide structure is obtained directly through one-step reduction of a sulfur-containing precursor. The sulfur is uniformly dispersed in the catalyst, existing as a combination of S^{2-} and thiolate species with a high concentration (S/Mo = 2.18). This unique composition contributes to the catalyst exceptional stability in air and its high reactivity in hydrodesulfurization, hydrodechlorination, and hydrogenation of nitrobenzene. Notably, the MoP-S catalyst, which is exposed to air for up to 150 days after reduction, exhibits comparable activity to the catalyst prepared through in situ reduction, in contrast to the common phosphosulfide layer of MoP-T obtained through reduction-H_2S passivation. This method is expected to have broad applications in the field of transition metal phosphides, enabling easy setup and accelerating the exploration of new reactivity.

Experimental Section

Catalyst preparation

To prepare the sulfur-containing precursor for sulfur modified MoP (MoP-S, Table 1), a solution of PCl_3 (6.60 mL, 0.0756 mol) was slowly added dropwise into a mixture of $(NH_4)_2S$ (22.0 g) in deionized water (50 mL) with continuous stirring in an ice bath. Another

solution of 3.8 g $(NH_4)_6Mo_7O_{24}\cdot 4H_2O$ in 10 mL of ammonia water was then added dropwise to the former mix solution under stirring for 1 h to yield an emulsion. The emulsion was further cooled in a refrigerator for 18 h to allow complete precipitation. Finally, the solid was collected by filtration, washed with ethanol and water, after drying at 120 °C for 8 h a black powder of sulfur-containing precursor was obtained.

For comparison, the phosphate precursor of MoP was prepared using a co-precipitation method.[25] An aqueous solution of 3.90 g $(NH_4)_6Mo_7O_{24}\cdot 4H_2O$ in 10 mL deionized water was added to a solution of 3.0 g $(NH_4)_2HPO_4$ in 10 mL deionized water with continuous stirring. The resulting precipitate was stirred until the water evaporated, yielding a solid product. The solid was then dried at 120 °C for 12 hours and calcined at 500 °C for 3 hours, resulting in the final oxidic precursor with a Mo/P molar ratio of 1. The phosphate precursor was further transformed into MoP using temperature programmed reduction method. The precursor was subjected to reduction in a flowing H_2 stream at a rate of 100 mL/min. The temperature was rapidly increased from room temperature to 120 °C and maintained for 1 hour, followed by heating to 400 °C at a rate of 5 °C/min and holding for 1 hour. Finally, the temperature was increased at a rate of 1 °C/min to 650 °C and held at 650 °C for 3 hours to obtain the active phase, referred to as MoP-T (Table 1).

Catalyst characterization

Considering the susceptibility of metal phosphide to oxidation upon exposure to air, all the reduced samples were passivated with a 0.5 % (volume) O_2 in Ar before being removed from the reactor for characterization. The crystallized phases of the catalyst were analyzed using X-ray diffraction (XRD) on an Empyrean PANalytical X-ray diffractometer equipped with Cu Kα radiation (λ = 1.54056 Å) at room temperature. The 2θ range was set from 5° to 90° with a step size of 0.02°. For surface analysis, the signals of surface elements were detected by the Energy-Dispersive X-ray spectroscopy (EDX) (Oxford INCA Energy IE350) mapping method. The particle size and morphology of the samples were observed using a transmission electron microscope (TEM, FEI Tecnai G2 F20) operating at 200 kV. X-ray photoelectron spectroscopy (XPS) was utilized to analyze the change of the coordination state of surface element measured by Thermo Scientific K-Alpha equipment, and the binding energy values were corrected for charging effect by referring to the adventitious C1s line at 284.8 eV. The metal content in the samples was determined using an X-ray fluorescence (XRF) spectrometer (ELEMENTAR Vario ELIII) with an uncertainty of 3 %. The Brunauer-Emmett-Teller (BET) surface area was calculated from the N_2 adsorption isotherms measured at −196 °C on a Micrometerics ASAP2020 system.

Catalytic tests

In the in situ experiments, the HDC of $CHClF_2$ and HDS of DBT were conducted in a fixed-bed stainless steel reactor with an inner diameter of 1.0 cm. The precursors of different MoP catalysts were pelleted, crushed, and sieved to 40–60 mesh. Prior to the reaction, 3 mL of prepared precursor was loaded into the reactor and converted into metal phosphide using an in situ H_2 TPR procedure. Subsequently, the temperature and total pressure were adjusted to the specified values as listed in Table S1, which provides an overview of the reaction conditions for each reaction. The HDC reaction products were analyzed offline by a gas chromatograph (SICT GC-2000III) equipped with a flame ionization detector (FID) and a GS-GASPRO capillary column (60 m×0.32 mm). HDS reaction products were analyzed offline by an Agilent-6890 N gas chromatograph equipped with an HP-5 column and a flame ionization detector.

In the ex situ experiments, the 40–60 mesh precursors converted into metal phosphide using a U-shaped quartz tube firstly, which subjected to the same heating procedure as in the in situ experiments under a H_2 atmosphere. After the temperature cooled down to room temperature, the samples were collected directly without undergoing any passivation process. Part of MoP-T samples obtained in this method were further treated with a 10.0 vol.% H_2S/H_2 mixture, and these samples were denoted as MoP-T-S (Table 1). The HDC reactions for those different samples were initiated immediately after heating the reactor to the target temperature. Additionally, the hydrogenation of nitrobenzene was employed for evaluation purposes. Typically, in this experiment, 1 mmol of nitrobenzene, 50 mg of the catalyst, and 10 mL of ethanol were introduced into a Parr autoclave equipped with mechanical agitation. The autoclave was purged with H_2 five times and then pressurized to 0.5 MPa with H_2. The mixture was stirred at 1000 rpm and maintained at a temperature of 50 °C. After the reactions, the products were separated from the catalyst and subsequently analyzed offline using an Agilent-6890N gas chromatograph equipped with an HP-5 column and a flame ionization detector.

Acknowledgements

We are grateful to financial support by China Scholarship Council (CSC, No. 202205290002), National Natural Science Foundation of China (No. 21902124), Natural Science Basic Research Planning Shaanxi Province of China (No. 2020JQ-983), and China Postdoctoral Science Foundation (No. 2019 M663848).

Conflict of Interests

The authors declare no conflict of interest.

Data Availability Statement

The data that support the findings of this study are available from the corresponding author upon reasonable request.

Keywords: air-insensitive · doping · heterogeneous catalysis · hydrofining · molybdenum phosphosulfide

[1] a) S. T. Oyama, T. Gott, H. Zhao, Y.-K. Lee, *Catal. Today* **2009**, *143*, 94–107; b) S. T. Oyama, P. Clark, X. Wang, T. Shido, Y. Iwasawa, S. Hayashi, J. M. Ramallolopez, F. G. Requejo, *J. Phys. Chem. B* **2002**, *106*, 1913–1920.
[2] a) X. Li, Y. Zhang, A. Wang, Y. Wang, Y. Hu, *Catal. Commun.* **2010**, *11*, 1129–1132; b) M. Lu, A. Wang, X. Li, X. Duan, Y. Teng, Y. Wang, C. Song, Y. Hu, *Energy Fuels* **2007**, *21*, 554–560; c) Z. Yu, Y. Wang, Z. Sun, X. Li, A. Wang, D. M. Camaioni, J. A. Lercher, *Green Chem.* **2018**, *20*, 609–619; d) W. Han, X. Li, B. Liu, L. Li, H. Tang, Y. Li, C. Lu, X. Li, *Chem. Commun.* **2019**, *55*, 9279–9282.
[3] a) J. Kibsgaard, T. F. Jaramillo, *Angew. Chem. Int. Ed.* **2014**, *53*, 14433–14437; b) Y. Xu, R. Wu, J. Zhang, Y. Shi, B. Zhang, *Chem. Commun.* **2013**, *49*, 6656–6658.

[4] M. S. Duyar, C. Tsai, J. L. Snider, J. A. Singh, A. Gallo, J. S. Yoo, A. J. Medford, F. Abild-Pedersen, F. Studt, J. Kibsgaard, S. F. Bent, J. K. Nørskov, T. F. Jaramillo, *Angew. Chem.* **2018**, *130*, 15265–15270.
[5] J.-y. Tang, D. Yang, W.-g. Zhou, R.-t. Guo, W.-g. Pan, C.-y. Huang, *J. Catal.* **2019**, *370*, 79–87.
[6] a) R. Prins, M. E. Bussell, *Catal. Lett.* **2012**, *142*, 1413–1436; b) X. Li, X. H. Wang, Y. Nie, B. X. Tao, Y. X. Yang, W. H. Guo, J. Zhang, Z. Cai, Y. Ling, W. Liu, H. Q. Luo, N. B. Li, *J. Catal.* **2020**, *382*, 228–236.
[7] a) C.-C. Weng, J.-T. Ren, Z.-Y. Yuan, *ChemSusChem* **2020**, *13*, 3357–3375; b) W. Bi, L. Zhang, Z. Sun, X. Li, T. Jin, X. Wu, Q. Zhang, Y. Luo, C. Wu, Y. Xie, *ACS Catal.* **2016**, *6*, 4253–4257; c) Z. Xing, Q. Liu, A. M. Asiri, X. Sun, *Adv. Mater.* **2014**, *26*, 5702–5707.
[8] S. Sloboshanin, R. K. Gebhardt, J. A. Schaefer, T. Chassé, *Surf. Sci.* **1999**, *431*, 252–259.
[9] X. Duan, Y. Teng, A. Wang, V. M. Kogan, X. Li, Y. Wang, *J. Catal.* **2009**, *261*, 232–240.
[10] Y. Teng, A. Wang, X. Li, J. Xie, Y. Wang, Y. Hu, *J. Catal.* **2009**, *266*, 369–379.
[11] a) J. Bai, X. Li, A. Wang, R. Prins, Y. Wang, *J. Catal.* **2013**, *300*, 197–200; b) X. Zhou, X. Li, R. Prins, A. Wang, L. Wang, S. Liu, Q. Sheng, *J. Catal.* **2020**, *383*, 331–342; c) S. T. Oyama, X. Wang, Y.-K. Lee, K. Bando, F. G. Requejo, *J. Catal.* **2002**, *210*, 207–217.
[12] G. Li, L. Zhao, H. Zhu, X. Liu, H. Ma, Y. Yu, W. Guo, *Phys. Chem. Chem. Phys.* **2017**, *19*, 17449–17460.
[13] S. Tian, X. Li, A. Wang, R. Prins, Y. Chen, Y. Hu, *Angew. Chem. Int. Ed.* **2016**, *55*, 4030–4034.
[14] W. Li, B. Dhandapani, S. T. Oyama, *Chem. Lett.* **1998**, *27*, 207–208.
[15] X. Tian, P. Li, T. Wang, *Mol. Catal.* **2019**, *464*, 57–62.
[16] D. C. Phillips, S. J. Sawhill, R. Self, M. E. Bussell, *J. Catal.* **2002**, *207*, 266–273.
[17] D. S. Zingg, L. E. Makovsky, R. E. Tischer, F. R. Brown, D. M. Hercules, *J. Phys. Chem.* **1980**, *84*, 2898–2906.
[18] I. I. Abu, K. J. Smith, *J. Catal.* **2006**, *241*, 356–366.
[19] H. Al-Kandari, F. Al-Kharafi, A. Katrib, *Catal. Commun.* **2008**, *9*, 847–852.
[20] B. V. R. Chowdari, K. L. Tan, W. T. Chia, R. Gopalakrishnan, *J. Non-Cryst. Solids* **1991**, *128*, 18–29.
[21] P. Clark, X. Wang, S. T. Oyama, *J. Catal.* **2002**, *207*, 256–265.
[22] X. Li, Z. Sun, A. Wang, X. Yang, Y. Wang, *Appl. Catal. A* **2012**, *417–418*, 19–25.
[23] Y. Li, R. A. van Santen, T. Weber, *J. Solid State Chem.* **2008**, *181*, 3151–3162.
[24] M. Piacentini, F. S. Khumalo, C. G. Olson, J. W. Anderegg, D. W. Lynch, *Chem. Phys.* **1982**, *65*, 289–304.
[25] J. Bai, X. Li, A. Wang, R. Prins, Y. Wang, *J. Catal.* **2012**, *287*, 161–169.
[26] Y. Han, G. Gu, J. Sun, W. Wang, H. Wan, Z. Xu, S. Zheng, *Appl. Surf. Sci.* **2015**, *355*, 183–190.
[27] A. Morato, C. Alonso, F. Medina, P. Salagre, J. E. Sueiras, R. Terrado, A. Giralt, *Appl. Catal. B* **1999**, *23*, 175–185.
[28] M. A. R. Anjum, J. S. Lee, *ACS Catal.* **2017**, *7*, 3030–3038.
[29] a) J. Chang, K. Li, Z. Wu, J. Ge, C. Liu, W. Xing, *ACS Appl. Mater. Interfaces* **2018**, *10*, 26303–26311; b) G. Ali, M. A. R. Anjum, S. Mehboob, M. Akbar, J. S. Lee, K. Y. Chung, *Int. J. Energy Res.* **2022**, *46*, 8452–8463.
[30] P. A. Clark, S. T. Oyama, *J. Catal.* **2003**, *218*, 78–87.

Manuscript received: September 4, 2023
Revised manuscript received: October 23, 2023
Accepted manuscript online: November 2, 2023
Version of record online: November 27, 2023